ISSN 0015-4628, Fluid Dynamics, 2022, Vol. 57, No. 3, pp. 387–400. © Pleiades Publishing, Ltd., 2022.
Russian Text © The Author(s), 2022, published in Izvestiya RAN. Mekhanika Zhidkosti i Gaza, 2022, Vol. 57, No. 3, pp. 135–150.

Increasing Flow Complexity in Time-Dependent Modulated Ferrofluidic Couette Flow

S. Altmeyer[a,*]

[a]*Castelldefels School of Telecom and Aerospace Engineering (EETAC), Universitat Politècnica de Catalanya, 08860 Barcelona, Spain*

**e-mail: sebastian.andreas.altmeyer@upc.edu*

Received December 2, 2021; revised December 21, 2021; accepted December 21, 2021

Abstract—We present numerical simulations of ferrofluidic Couette flow in between counter-rotating cylinders with a spatially homogeneous magnetic field but subject to *time-periodic* modulation. Such a modulation can lead to a significant inner Reynolds number (Re_i) enhancement for primary bifurcating solutions, for either helical or toroidal flow structures. Moreover, the external introduced modulation frequency renders the different solutions to step up one level in the hierarchy of complexity. Fixed point solutions become limit cycles and limit cycles become 2-tori. Moreover, for sufficiently strong modulation amplitudes of the magnetic field stability can be exchanged between primary bifurcating spiral and ribbon solutions, both appearing at a common threshold. In addition, a stable bifurcation branch with direct connection of ribbon and Taylor vortices via wavy Taylor vortices is found.

Keywords: Navier–Stokes equations, ferrofluids, modulated magnetic field, bifurcation scenario, time-periodic forcing, direct numerical simulation, computational fluid dynamics

DOI: 10.1134/S0015462822030016

A benchmark example to investigate problems of instability, non-linear behavior, and pattern formation is the motion of an incompressible viscous fluid between concentric rotating cylinders (Taylor–Couette system, TCS) [1, 2]. Motivated by widespread technological importance of such a flow (e.g. in pumping processes), various works have been shown that TCS with an external temporal forcing is a paradigm problem to study the control of flow instabilities.

Classical such an external forcing typically enters mechanical into the system via modification in the boundary conditions, e.g., harmonically modulated rotations of either the inner or outer cylinder (or both), harmonic oscillations of one cylinder in the axial direction, pulsation, etc. [3–12]. Already the early experimental works by Donnelly *et al.* [7, 8] detected a stabilization effect resulting from such forcing. Since those days this problem has served as model to gain understanding into time-periodic forcing and therefrom resulting effects.

Considering a magnetic fluid, e.g., a ferrofluid [13–15] offers the great advantage to maintain a stationary setup while introducing any periodic forcing directly into the fluid within the bulk. To date numerous numerical and experimental studies for ferrofluidic Couette flows under static magnetic fields have been performed. These focused on various aspects, as different field orientations, agglomeration, internal magnetization, torque measurements, etc. [16–30]. The common conclusion of all these works is the fact that a static magnetic field, independently of its orientation stabilizes the basic state (Circular Couette flow, CCF), i.e., moving the bifurcation threshold of the primary instability to greater values of the respective control parameter (e.g., the inner Reynolds number Re_i).

To date the studies of ferrofluids under alternating magnetic fields are relatively rare and if so special attention is given to viscosity effects [31] and heat behavior [32, 33]. However, analogosly to static fields, the modulated fields with sufficiently high modulation frequency stabilize the CCF basic state [15, 31] and can provide an accurate control parameter to balance the system to be either sub- or supercritical [15]. Different works, mainly focused on the use of temporal modulation in heating binary fluids and ferrofluids [34–36], illustrated that the parameter modulation in the hydrodynamic systems causes the parametric resonance. Thereby three types of response are possible with respect to the external forcing parameter. A *synchronous* response in the case, when the system response follows the external forcing, i.e., the frequency of oscillating flow coincides with the frequency, associated with the excitation period. A *subhar-*

monic response, if the oscillations of the system characteristics have a frequency twice the external forcing, i.e., half a period. A quasi-periodic response in the case, when the flow oscillations may have two different and *not rationally related* characteristic frequencies [37].

There is raising interest in using modulated magnetic fields for the flow control due to their highly desired features and huge variety in applications. One field with growing interest and great opportunities are medical applications. Here ferrofluids can be used as carriers of drugs, which then, after injection into a blood vessel can be concentrated at a desired position by applying a strong magnetic field gradient [38]. Other opportunity lies in the therapy technique for cancer treatment by hyperthermia. Enriching fluid particles that are marked with tracer substances in the tumor tissue, an alternating magnetic field can be applied, while the energy losses due to magnetization change in the particles can be used to heat up the tissue [39]. This allows avoiding undesired side effects to other organs while destroying the tumor.

For here studied pure axial (modulated) magnetic field, the classical flow structures appearing in TCS are preserved. Thus, primary stationary bifurcating solutions are toroidally closed Taylor vortex flow (TVF) [1, 40, 41] and the two axisymmetric degenerated oscillatory spiral vortices (spiral vortex flow, SPI) [40, 41] with left or right winding helicoidal vortices appearing in symmetry breaking Hopf bifurcation. Together with the latter, also ribbon (RIB) state bifurcates, which can be seen as a non-linear superposition of the two oppositely propagating SPIs to an axially standing wave. The stability of TVF and SPI at onset is regulated by the order of their appearance depending on the given control parameter, e.g., outer cylinder rotation speed or as in the present case the modulation amplitude of the magnetic field.

From the dynamical system point of view the classical TVF, appearing in circle pitchfork bifurcation, represents a fixed point solution, while the classical SPI and RIB correspond to limit cycle solutions [2, 42, 43]. However, this changes in the presence of a modulated magnetic field as the flow dynamics increases in complexity. Here the additional modulation frequency Ω_H increases the dimension of the underlying manifold by one. Thus, the former stationary (fixed point) solution becomes periodic limit cycles (here TVF), as well as the former periodic solution becomes a quasi-periodic solution (here SPI, RIB, and wTVF). Moreover, sufficiently strong modulated magnetic fields can exchange stability between SPI and RIB and with this also stabilize the whole wavy Taylor vortex (wTVF) branch, as part of the transition process between different topological (helical and azimuthal closed) structures. Earlier studies revealed this as "jump bifurcation" [44, 45].

1. NUMERICAL METHODS

1.1. System Setting

We consider a standard TCS (Fig. 1) consisting of two concentric, independently rotating cylinders and the gap between them filled with an incompressible, isothermal, homogeneous, mono-dispersed ferrofluid of kinematic viscosity ν and density ρ. The inner (outer) cylinder has radius $R_i(R_o)$ and rotates with the angular velocity $\omega_i(\omega_o)$. In the axial (z) direction we use periodic boundary conditions corresponding to a fixed axial wavenumber $k = 3.927$, while the no-slip boundary conditions are used on the cylinder surfaces. Using the cylindrical coordinate system (r, θ, z) the system can be characterized by the velocity field and the corresponding vorticity field $u=(u,v,w)$, $\nabla \times u = (\xi, \eta, \zeta)$. In the present work the radius ratio of the cylinders is kept fixed at $R_i/R_o = 0.5$. Further a counter-rotating system setup is studied with fixed outer Reynolds number $Re_o = -125$. The time and length scales are made dimensionless by the diffusion time d^2/ν and the gap width d and the pressure in the fluid is normalized by $\rho\nu^2/d^2$. Worth mentioning that here we use the assumption of a single-component ferrofluid neglecting diffusion of nanoparticles, which also may play a role and affect the flow dynamics.

The periodical forcing is applied via a sinusoidal modulation signal to the external magnetic field, which is orientated parallel to the system symmetry (z) axis, uniform in space and harmonic in time $H_z = [H_S + H_M \sin(\Omega_H t)]e_z$. Note that in the static case such a *pure* axially-orientated magnetic field *preserves* the basic system symmetry (see Subsection 1.3), it only shifts the stability thresholds as reported in the earlier studies [23–25]. The magnetic field H and the magnetization M are conveniently normalized by the quantity $\sqrt{\rho/\mu_0}\nu/d$ with free space permeability μ_0.

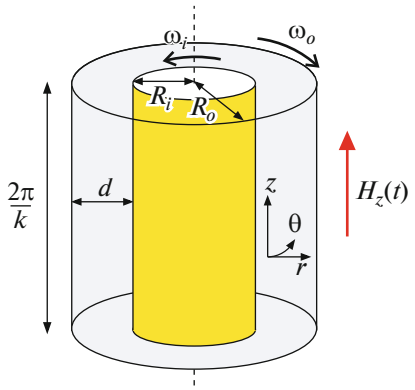

Fig. 1. Schematic of the Taylor–Couette system (TCS) with an external applied spatial homogeneous but time-dependent magnetic field $H_z(t) = [H_S + H_M \sin(\Omega_H t)]e_z$.

1.2. Ferrohydrodynamical Equation of Motion

The non-dimensionalized hydrodynamical equations [25, 27, 46] are derived from

$$(\partial_t + u\times\nabla)u - \nabla^2 u + \nabla p = (M\times\nabla)H + \frac{1}{2}\nabla\times(M\times H),$$
$$\nabla\times u = 0. \tag{1.1}$$

The velocity fields on the cylindrical surfaces are $u(r_i,\theta,z) = (0,\mathrm{Re},0)$ and $u(r_o,\theta,z) = (0,0,0)$, with the inner and outer Reynolds numbers $\mathrm{Re}_{i,o} = \omega_{i,o}r_{i,o}d/\nu$, where $r_i = R_i/(R_o - R_i)$ and $r_o = R_o/(R_o - R_i)$ are the non-dimensionalized inner and outer cylinder radii, respectively.

To solve Eq. (1.1) one needs a further equation describing the magnetization of the ferrofluid. Consider equilibrium magnetization of an unperturbed state with homogeneously magnetized ferrofluid at rest and the mean magnetic moment orientated in the direction of the magnetic field: $M^{\mathrm{eq}} = \chi H$. The magnetic susceptibility χ of the ferrofluid can be approximated with Langevin's formula [47]. The initial value χ is set to be 0.9 with use of a linear magnetization law. The ferrofluid studied corresponds to APG933 (Ferrofluidics) [48, 49]. We consider the near-equilibrium approximations of Niklas [19, 50] with small $\|M - M^{\mathrm{eq}}\|$ and small magnetic relaxation time τ: $|\nabla\times u|\tau \ll 1$. Using these approximations, one can obtain [27] the following magnetization equation

$$M - M^{\mathrm{eq}} = c_N^2\left(\frac{1}{2}\nabla\times u\times H + \lambda_2\mathbb{S}H\right), \tag{1.2}$$

where

$$c_N^2 = \tau/(1/\chi + \tau\mu_0 H^2/6\mu\Phi) \tag{1.3}$$

is the Niklas coefficient [19], μ is the dynamic viscosity, Φ is the volume fraction of the magnetic material, $\mathbb{S}$ is the symmetric component of the velocity gradient tensor [27, 46], and λ_2 is the material-dependent transport coefficient [46], which we choose to be $\lambda_2 = 4/5$ [30, 46, 51, 52]. Using Eq. (1.2) we can eliminate the magnetization from Eq. (1.1) to obtain the following ferro-hydrodynamical equations of motion [25, 27, 46]

$$(\partial_t + u\cdot\nabla)u - \nabla^2 u + \nabla p_M = -\frac{s_z^2}{2}\left[H\nabla\cdot\left(F + \frac{4}{5}\mathbb{S}H\right) + H\times\nabla\times\left(F + \frac{4}{5}\mathbb{S}H\right)\right], \tag{1.4}$$

where $F = (\nabla\times u/2)\times H$, p_M is the dynamic pressure incorporating all magnetic terms that can be expressed as gradients, and s_z is the Niklas parameter [Eq. (1.6)]. To the leading order, the internal magnetic field in the ferrofluid can be approximated as the externally imposed field [25], which is reasonable

for obtaining dynamical solutions of the magnetically driven fluid motion. Equation (1.4) can then be simplified as follows:

$$(\partial_t + u\cdot\nabla)u - \nabla^2 u + \nabla p_M = s_z^2\left\{\nabla^2 u - \frac{4}{5}[\nabla\cdot(\mathbb{S}H)]\right. \tag{1.5}$$

$$\left. - H\times\left[\frac{1}{2}\nabla\times(\nabla\times u\times H) - H\times(\nabla^2 u) + \frac{4}{5}\nabla\times(\mathbb{S}H)\right]\right\}.$$

This way, the effect of the magnetic field (here homogeneous but periodically alternating with $H_z = [H_S + H_M \sin(\Omega_H t)]e_z$) and all the magnetic properties of the ferrofluid on the velocity field can be characterized by a single (here time-dependent) Niklas parameter [19]

$$s_z(t) = \sqrt{c_N}H_z = \sqrt{c_N}[H_S + H_M \sin(\Omega_H t)] \tag{1.6}$$

$$= s_{z,S} + s_{z,M}\sin(\Omega_H t),$$

with two *time-independent* control parameters

$$s_{z,S} = \sqrt{c_N}H_S \quad \text{and} \quad s_{z,M} = \sqrt{c_N}H_M. \tag{1.7}$$

$s_{z,S}$ being the *static contribution* of the driving, $s_{z,M}$ the *modulation amplitude*, and Ω_H the *modulation frequency*. In the present study we consider a pure modulated magnetic field (without any static contribution, $s_{z,S} = 0$) in the high frequency limit $\Omega_H = 0$, which means that the effects of inertia of the fluid can be neglected and the system basically sees an averaged magnetic field [15].

1.3. Symmetries

In absence of any periodic forcing the symmetry group of the Taylor–Couette problem is $O(2)\times SO(2)$ [2]. The basic state is invariant to a number of symmetries, whose actions on a general velocity field are as follows:

$$\begin{aligned} R_\Phi(u,v,w)(r,\theta,z) &= (u,v,w)(r,\theta+\Phi,z),\\ K_z(u,v,w)(r,\theta,z) &= (u,v,-w)(r,\theta,-z),\\ T_\alpha(u,v,w)(r,\theta,z) &= (u,v,w)(r,\theta,z+\alpha). \end{aligned} \tag{1.8}$$

The $SO(2)$ symmetry comes from rotations around the axis. $O(2)\times SO(2)$ remains the symmetry group for the periodically forced system. While $SO(2)$ remains unaffected by the modulation, the axial reflection symmetry is broken and therefore is no longer a symmetry of the problem. Instead, composing with a half-period time translation one obtains a glide-time symmetry G of the system. This symmetry, together with axial translations, still gives the symmetry group $O(2)$. Explicit acting on the velocity fields, one obtains following expression of this symmetry (half-period-flip-symmetry),

$$G(u,v,w)[r,\theta,z,t] = (u,v,-w)[r,\theta,-z,t\acute{y}]. \tag{1.9}$$

With this R changes from the purely spatial symmetry to a space-time symmetry. A consequence of the space-time Z_2 symmetry generated by G implies a more complex bifurcation scenario, e.g., inhibiting period doubling via a simple negative eigenvalue $\mu = -1$ [4, 53].

1.4. Numerics

The ferrohydrodynamical equations of motion Eq. (1.4) can be solved [24, 25, 27] by combining a standard, second-order finite-difference scheme in (r, z) with the Fourier spectral decomposition in θ and (explicit) time splitting. The variables can be expressed as follows:

$$f(r,\theta,z,t) = \sum_{m=-m_{\max}}^{m_{\max}} f_m(r,z,t)e^{im\theta}, \tag{1.10}$$

where f denotes one of the variables $\{u, v, w, p\}$. For the parameter regimes considered, the choice of $m_{\max} = 16$ provides adequate accuracy. We use a uniform grid with the spacing $\delta r = \delta z = 0.02$ and the

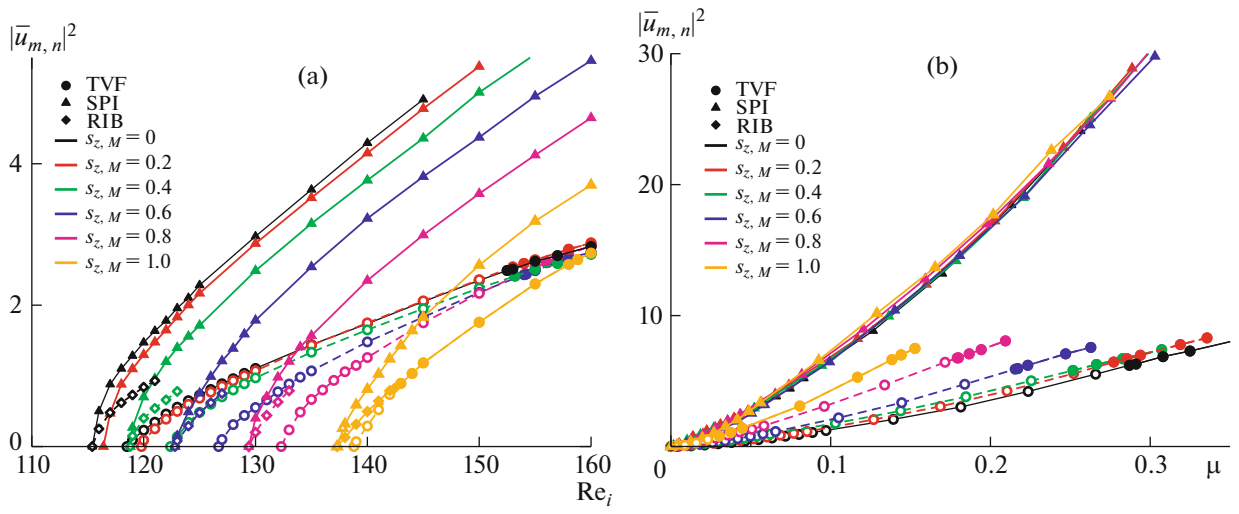

Fig. 2. Bifurcation diagram. Time averaged mode amplitudes $|\overline{u}_{m,n}|$ of (dominant) radial flow field amplitudes for TVF ($|\overline{u}_{0,1}|$, •) and SPI ($|\overline{u}_{1,1}|$, ▲) at mid gap for different modulation amplitudes $s_{z,M}$ in the magnetic fields versus (a) inner Reynolds number Re_i and (b) relative distance $\mu = \mathrm{Re}_i(s_{z,M})/\mathrm{Re}_{i,c}(s_{z,M}) - 1$, from the respective onset ($\mathrm{Re}_{i,c}(s_{z,M})$) for given modulation amplitudes $s_{z,M}$ in the magnetic fields. Solid and open symbols indicate the solution to be stable and unstable, respectively. SPI bifurcate stable for $s_{z,M} \lesssim 0.82$ and remain stable afterwards, while TVF bifurcates initially unstable and become stabilized for larger Re_i. Note for the seek of visibility the RIB branches are only shown close to onset. RIB bifurcate at a common threshold while both exchange stability at onset. Thus RIB appear stable for $s_{z,M} \gtrsim 0.82$. See also Fig. 7.

time steps $\delta t < 1/3800$. For diagnostic purposes, we also evaluate the complex mode amplitudes $f_{m,n}(r,t)$ obtained from the Fourier decomposition in the axial direction

$$f_m(r,z,t) = \sum_n f_{m,n}(r,t)e^{inkz}, \tag{1.11}$$

where $k = 2\pi d/\lambda$ is the axial wavenumber.

2. RESULTS

2.1. Bifurcation Behavior

In classical TCS, the primary solutions of TVF appear in a supercritical pitchfork of the revolution bifurcation breaking the translation symmetry T_α. TVF represent a steady axisymmetric family of solutions parameterized by their axial location, which visually appear as a pile of "fluid donuts." Meanwhile, SPI and RIB, appear in the $O(2)$ symmetry breaking Hopf bifurcation (eliminating K_z). From the dynamical point of view these correspond to fixed point and limit cycle solutions, respectively. However, the periodical forcing changes this "classical" scenario. In fact, it increases the underlying manifold by one dimension. Thus, TVF appear as a limit cycle solution, while SPI and RIB become only quasi-periodic solutions on a 2-torus. We will focus on this in more detail in Subsection 2.1.4.

2.1.1. Stability thresholds with variation in modulation amplitude $s_{z,M}$. Figure 2a shows the forward bifurcating branches of SPI (Δ) and TVF (○) solutions for different modulation amplitudes $s_{z,M}$ of the magnetic field as indicated. The onsets correspond to the critical curve with variation in the modulation amplitude $s_{z,M}$ (Fig. 7). The bifurcation thresholds for RIB and SPI coincide [2, 45, 54]. For all but $s_{z,M} = 1$ RIB are unstable at the onset, while SPI are stable.

Being supercritical for SPI, RIB, and TVF the dominant mode amplitudes $|\overline{u}_{1,1}|$ and $|\overline{u}_{0,1}|$ grow in the well-known square root manner. We note that here we use the time-averaged mode amplitudes $|\overline{u}_{m,n}|$; $|u_{m,n}|$ are time-periodic according to the modulation frequency Ω_H (cf. Fig. 5).

However, there are several obvious differences in the branches corresponding to the two different solutions. The bifurcation branches for SPI remain basically the same, they just become shifted together with the corresponding onset to greater Re_i with increasing $s_{z,M}$ (to the right in Fig. 2a). SPI remain *stable* in almost entire parameter range presented here. The TVF branches behave differently with increasing modulation amplitude. First of all, TVF are *unstable* close to their onsets and become stabilized for greater Re_i. Second, being supercritical, the slopes with increasing Re_i are much smaller than those for SPI (at least for small and moderate values $s_{z,M}$). Third, these slopes continuously steepen with increasing $s_{z,M}$. This modification in the bifurcation characteristics is best visible by rescaling the bifurcation scenario with the corresponding critical onsets (Fig. 2b). All curves for SPI fall together (i.e., on top of each other). On the other side, the mode amplitudes for TVF with increasing modulation amplitudes $s_{z,M}$ grow noticeably faster, and thus the corresponding slopes steepen. Thus, SPIs seem to be more robust against greater modulation amplitudes, i.e., their internal flow dynamics remains the same.

As a result, one can say that an increase in the modulation amplitude $s_{z,M}$ moves the onset of all primary instabilities SPI, RIB, and TVF to the greater values of the control parameter Re_i (to the right in Fig. 2a) and with this stabilizes the CCF basic state against any primary appearing instability. Although the magnitude of stabilization is different, it does not change the bifurcation order (for here considered parameters). Similar numerical and experimental observations have been already found for increasing field strength in static magnetic fields [22–24] and recently for TVF in modulated magnetic fields [15] with the outer cylinder at rest. For sufficiently large modulation amplitudes the stability in the primary bifurcating solution is exchanged from SPI towards RIB.

2.1.2. Stable connection RIB – wTVF. Large modulation amplitudes $s_{z,M} = 1$ not only transfer stability between two primary bifurcating solutions, from SPI towards RIB (cf Fig. 2) but they can even further stabilize the whole bifurcation branch connecting RIB with TVF via wTVF [44, 45].

To see this phenomenon, Fig. 3 illustrates the stable (solid lines with closed symbols) and unstable (dashed lines with open symbols) bifurcation branches of TVF (blue circles), SPI (red triangles), RIB (green lozenges), and wTVF (black squares) versus Re_i in absence of any magnetic field $s_{z,M} = 0$ (*a*) and at large modulation amplitudes $s_{z,M} = 1$ (*b*), respectively. Corresponding parameters are also indicated by two arrows (*a*) and (*b*) in the phase diagram of Fig. 7. Shown are (a) the modal kinetic energy $E_{\mathrm{kin}} = \sum_m E_m = \frac{1}{2}\sum_m \int_0^{2\pi}\int_{-\Gamma/2}^{\Gamma/2}\int_{r_i}^{r_0} u_m u_m^* r dr dz d\theta$ (where u_m (u_m^*) is the mth (complex conjugate) Fourier mode of the velocity field) and (b) the mode amplitudes $|u_{m,n}|$.

The bifurcation scenario in absence of any magnetic field (1.3) was discussed before and is here mainly presented as reminder and comparison. For detailed description we refer to the earlier work [45]. In short, with decreasing Re_i stable wTVF bifurcate secondarily out of TVF, which then lose their stability. With the wTVF approaching the unstable RIB branch, the wTVF become unstable and "jump" up towards the only stable SPI branch [44, 45] (indicated by vertical arrows in Fig. 3 (1)).

For large modulation amplitudes $s_{z,M} = 1$ at a first glance the bifurcation scenario looks qualitatively very similar, while it is moved to greater Re_i due to the former discussed stabilization effect of a modulated field. However, more crucial is the fact that all the solutions move up in complexity (by one dimension) due to the external forcing introduced by the modulated magnetic field (see below). Further significant difference is the fact that for $s_{z,M} = 1$ *no* "jump" appears and instead the wTVF branch connects *directly* to RIB and transfers the stability from one to the other (Fig. 3b).

In absence of any magnetic field, the modal kinetic energy E_{kin} for the different solutions SPI, RIB, and TVF shows a convex behavior with increasing Re_i, while E_{kin} at the onset of TVF being greater than the one for SPI and RIB (at the same Re_i). As to expect, E_{kin} for wTVF is slightly greater than for (unstable) TVF, due to the more complex flow dynamics, with additional helical contributions. Qualitatively, for large modulation amplitude $s_{z,M}$ the variation of E_{kin} with Re_i is very similar. However, the curves for the different solutions are less convex and especially at the onset they show mainly linear behavior. Further the energy E_{kin} for the two helical solutions SPI and RIB lies above the two toroidally ones TVF and wTVF.

2.1.3. Flow characteristics. Following the wTVF bifurcation branch from TVF towards the stable RIB branch one observes that the flow dynamics shows an increase in waviness (see Fig. 4 (2, 3, 4)), i.e., the amplitude in the helical modes $u_{1,\pm}$ increases while the corresponding one in the azimuthal dominant modes $u_{0,\pm1}$ continuously decreases (Fig. 3b). At some point the helical modes $u_{1,\pm1}$ (Fig. 3a) even become

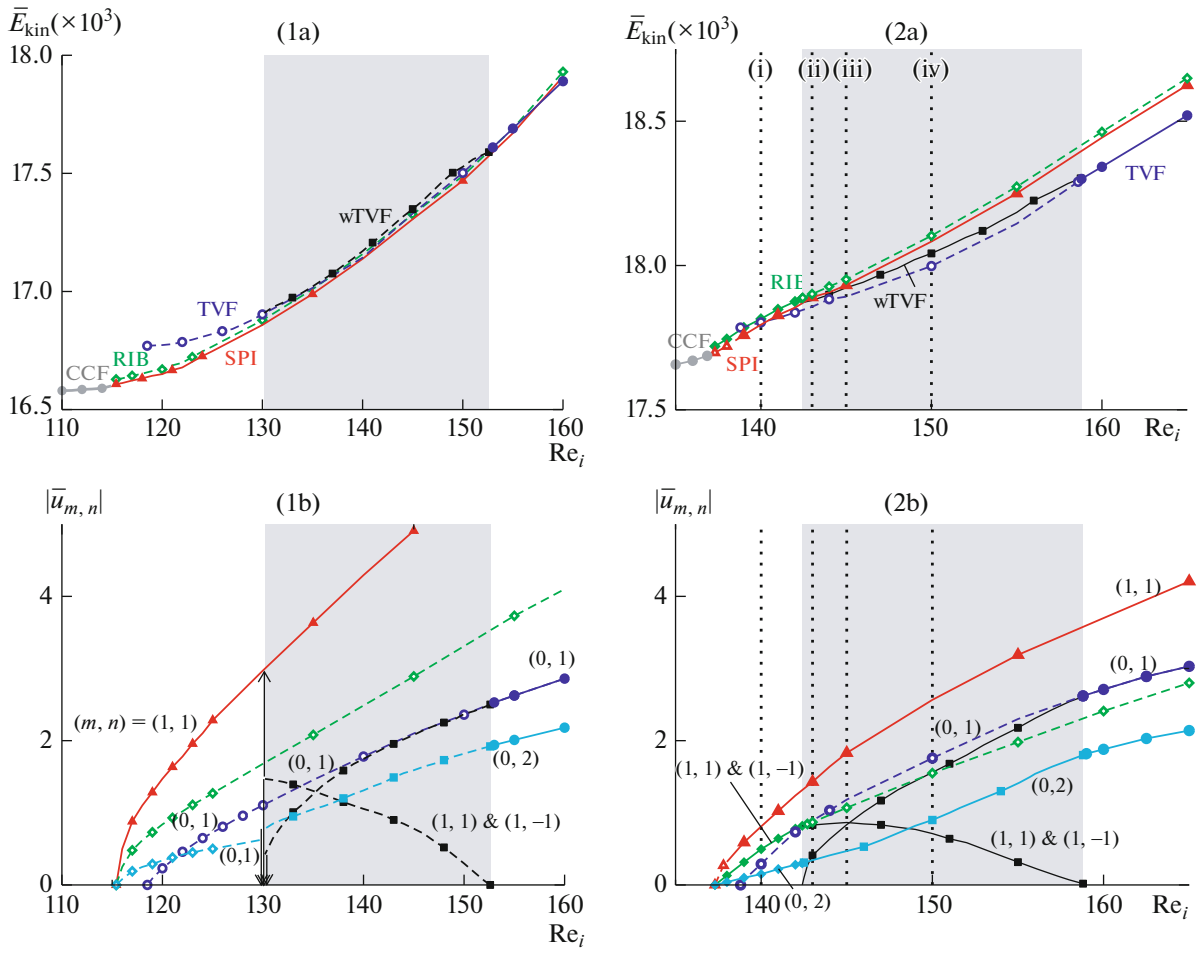

Fig. 3. Bifurcation diagrams for different vortex structures versus Re_i for (1) $s_{z,M} = 0$ and (2) $s_{z,M} = 1$ (cf. arrows in Fig. 7). Full (dashed) lines with filled (open) symbols refer to stable (unstable) solutions. Shown are (a) modal kinetic energy $E_{\rm kin}$ and (b) dominant radial flow field amplitudes $|u_{m,n}|$ at mid-gap for TVF $(m,n) = (0,1)$, SPI $(m,n) = (1,1)$, RIB $(|u_{1,1}| = |u_{1,-1}|)$, and wTVF. Characteristic feature for the wavy solution is $u_{0,1} \neq 0$ and $u_{1,\pm 1} = 0$ while $u_{0,1}^{\rm SPI} = 0 = u_{1,\pm 1}^{\rm TVF}$. (i–iv) indicate parameter sets for which flow visualizations are shown in Fig. 4.

greater than the toroidal one. This holds for both scenarios, either if RIB are stable or unstable. With decreasing $u_{0,\pm 1}$ the vortex tubes within the azimuthal wTVF shrink together at distinct azimuthal positions ($\theta = \pi/4$) (Fig. 4(2c)). Eventually, when $u_{0,\pm 1}$ vanishes the vortex tubes disconnect resulting in RIB. To highlight the direct connection of wTVF and RIB branches Fig. 3(2b) also includes the modes $(0,\pm 2)$; while for $s_{z,M} = 0$ an according "jump" appears to zero (as $(0.\pm 1)$) when transition towards SPI, for $s_{z,M} = 1$ the mode smoothly continuous (no jump) from wTVF to RIB.

2.1.4. Increasing in complexity. To quantify the effects introduced by the field modulation amplitude $s_{z,M}$, Fig. 5 illustrates time series and the corresponding power spectral density (PSD) for the global measure $E_{\rm kin}$ and the local measure $\eta_{\pm} = (0, 0, \pm 0.25\Gamma)$ of different flow states as indicated. The PSD for TVF (Fig. 5(1)) highlights best the external field induced modulation frequency Ω_H, equally for the global quantity $E_{\rm kin}$ and the local quantity η_+. While classical TVF is a time independent stationary fixed point solution, here the time-modulated magnetic field renders TVF to be a limit cycle and therefore raises it one step in the hierarchy of complex solution. Thus, the PSD for TVF shows classical synchronous response [55]. For here considered field modulation frequency $\Omega_H = 100$ the resulting frequency f_H appearing in the limit cycle solution of TVF is $f_H = \Omega_H/2\pi = 15.916$ $(\Omega_H = 100)$, which is equivalent to

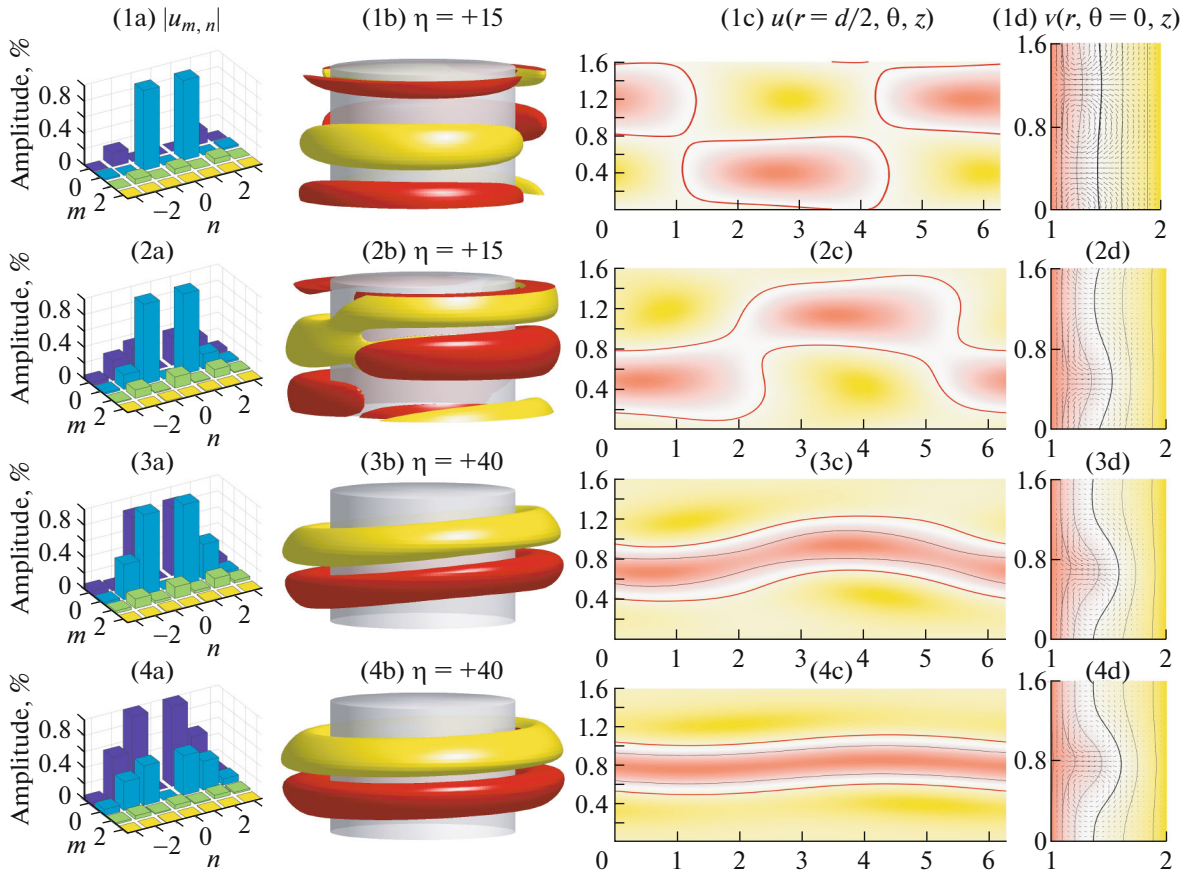

Fig. 4. Flow visualization of different stable flow structures along the RIB – wTVF connecting branch appearing with variation in Re_i. Snapshots of (1) RIB at $\mathrm{Re}_i = 0$, (2) wTVF at $\mathrm{Re}_i = 3$, (3) wTVF at $\mathrm{Re}_i = 5$, and (4) wTVF at $\mathrm{Re}_i = 0$ (corresponding parameters are indicated by vertical lines (i)–(iv) in Fig. 3). Shown are (a) Fourier spectrum (m,n), (b) isosurfaces of η [red (dark gray) and yellow (light gray) colors correspond to positive and negative values, respectively, with zero specified as white], (c) the radial velocity $u(\theta, z)$ on an unrolled cylindrical surface in the annulus at mid-gap [red (yellow) color indicates in (out) flow], and (d) vector plot $[u(r,z), w(r,z)]$ of the radial and axial velocity components (including the color-coded azimuthal velocity v).

the modulation period $\tau_H = 0.0628$. Similarly, also SPI and RIB, the classical limit cycle solutions (1-torus), raise to a more complex solution type. They become quasi-periodic solutions (2-tori) due to the intrinsic field induced frequency Ω_H. SPI and RIB (Fig. 5 (2,3)) share the main frequency (f_{SPI}, f_{RIB}) characterizing them as modulated rotating waves; note classical SPI and RIB are rotating waves, respectively. These are both the examples of quasiperiodic response [55]; for SPI the ratio $f_{\mathrm{SPI}}/f_{\mathrm{H}} = 3.354/15.916 = 0.2107$, while for RIB $f_{\mathrm{RIB}}/f_{\mathrm{H}} = 3.426/15.916 = 0.2152$. The modulation due to the time-dependent field is best visible in the corresponding time series of the local measures $\eta_{\pm}$ (insets in Figs. 5 (2b, 3b)). The corresponding PSDs of η_+ show all non-linear superposition of these two frequencies, while PSDs and time series of E_{kin} as global measure are much simpler. Although having almost identical frequencies, the peak in the PSDs for f_{RIB} is much smaller than for f_{SPI} which results from the fact that RIB are standing waves in the axial direction, while SPI are also axial propagating. For wTVF (Fig. 5 (4)) the time series of $\eta_{\pm}$ are very similar to RIB with the greater range and corresponding PSD shows a ratio about $f_H : f_{\mathrm{wTVF}} = 5:1$ ($f_{\mathrm{wTVF}}/f_{\mathrm{H}} = 3.221/15.916 = 0.2023$). In contrast to RIB, f_{wTVF} does not appear in the PSD of the global quantify E_{kin}, only in the PSD of the local quantity η_+. This results from the different nature of wTVF and SPI. wTVF is basically a TVF with azimuthal (helical) modulation, while RIB is a superposition of two pure helical SPIs with opposite winding direction but the same frequency f_{SPI}.

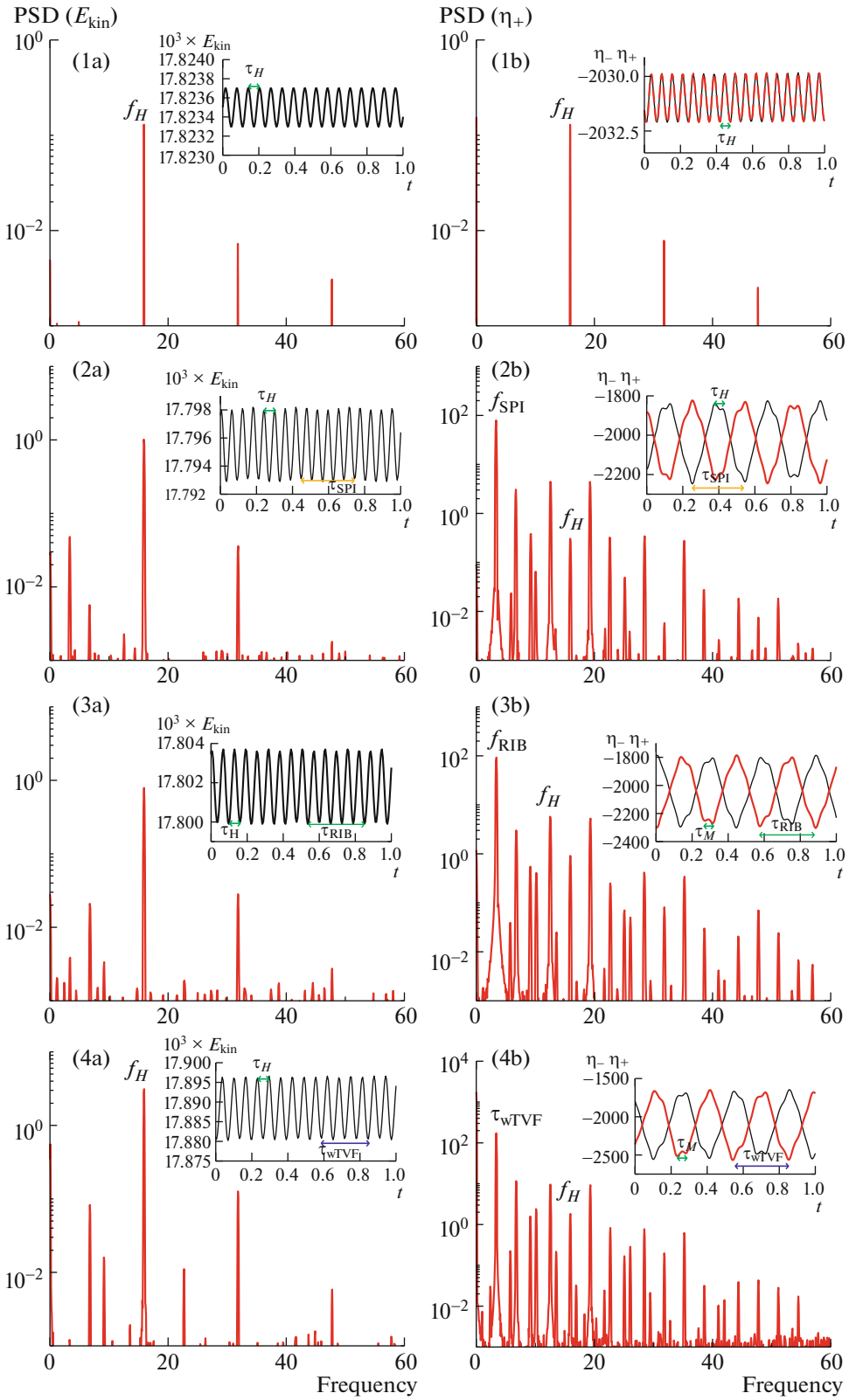

Fig. 5. Time series and power spectral density (PSD) of different flow structures with Re_i as indicated. PSD of (a) E_{kin} and (b) η_+ [$\eta_\pm = (0, 0, \pm 0.25\Gamma)$] for (1) TVF (unstable) at $\mathrm{Re}_i = 0, s_z = 1.0$) with $\tau_{\mathrm{TVF}} = \tau_H \approx 0.0628$ ($f_{\mathrm{TVF}} = f_H \approx 15.916$), (2) SPI at $\mathrm{Re}_i = 0, s_z = 1.0$ with $\tau_{\mathrm{SPI}} \approx 0.298$ ($f_{\mathrm{SPI}} \approx 3.354$), (3) RIB at $\mathrm{Re}_i = 0, s_z = 1.0$ with $\tau_{\mathrm{RIB}} \approx 0.292$ ($f_{\mathrm{RIB}} \approx 3.426$), (4) wTVF at $\mathrm{Re}_i = 3, s_z = 1.0$ with $\tau_{\mathrm{wTVF}} \approx 0.299$. Insets show time series of (a) E_{kin}, and (b) η_+ [red (gray)], η_- (black), respectively. Parameters are also indicated in Fig. 7

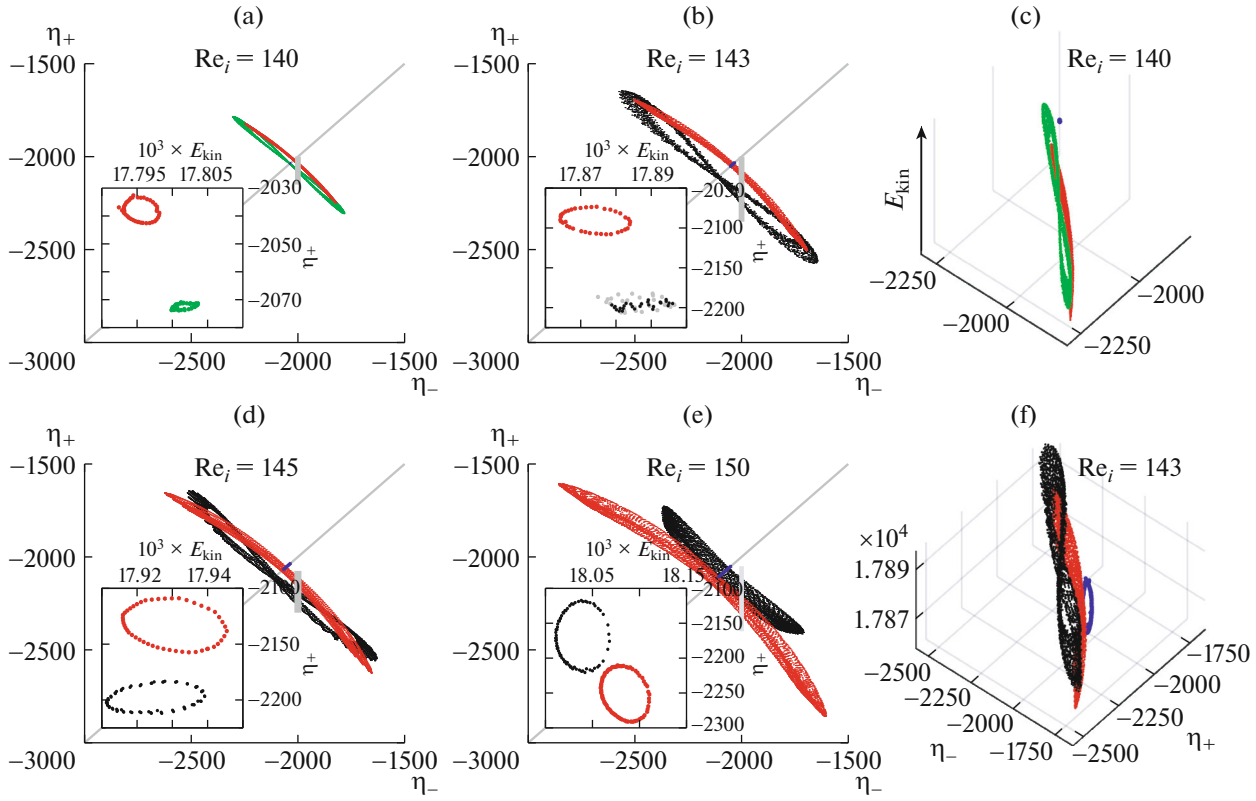

Fig. 6. (a–d) Phase portraits in (η_-, η_+) plane and (e, f) phase space dynamics in $(\eta_+, \eta_-, E_{kin})$ of TVF, SPI, RIB, and wTVF for Re$_i$ as indicated on (η_-, η_+) plane.

In order to visualize the change and evolution in flow dynamics with variation in Re$_i$, Fig. 6 illustrates the phase portraits of the different solutions TVF, SPI, RIB, and wTVF appearing along the transformation path over the (η_-, η_+) plane. In the (η_+, η_-) plane TVF solutions come to lie on the diagonal $\eta_+ = \eta_-$ line, i.e., topologically speaking this represents a degenerated limit cycle. However, the 3D visualization of $(\eta_+, \eta_-, E_{kin})$ (Figs. 6e, 6f) uncovers the limit cycle characteristic of TVF, which becomes more and more pronounced with increasing $s_{z,M}$.

Both, SPI and RIB representing modulated rotating waves and modulated standing waves, respectively, are symmetrically arranged with respect to the diagonal $\eta_- = \eta_+$. With increasing Re$_i$, i.e., becoming more supercritical a larger area in the phase space (η_-, η_+) is explored without any qualitative changes. While classically SPI and RIB are periodic limit cycle (1-torus) solutions, the additional time-dependent forcing increases their dimension by +1 which means that they appear now as quasi-periodic solutions, i.e., on a 2-torus invariant manifold. The insets in Figs. 6a–6d show the corresponding two-dimensional Poincaré sections (E_{kin}, η_+) at $\eta_- = 2000$ (marked by gray lines in (η_-, η_+) space), which results in closed circles for SPI, RIB, and TVF. With increasing Re$_i$ the phase portraits for all solutions SPI, RIB, and wTVF explore a wider range in the phase space (η_-, η_+), while wTVF moves towards greater values of $\eta_\pm$ (towards top right in Figs. 6a–6d) and SPI moves in opposite direction to smaller values of $\eta_\pm$ (towards bottom left in Figs. 6a–6d). Thereby all symmetries remain in place.

The TVF branch remains two-dimensional, preserving the reflection symmetry about the mid-plane. However, this symmetry is broken for the other solutions, SPI, RIB, and wTVF, which preserve a more complex shift reflection symmetry, that renders them to be fully three-dimensional.

2.2. Phase Diagram

As discussed previously (Fig. 2), an increase in the modulation amplitude $s_{z,M}$ stabilizes the system, i.e., the different instabilities appear at greater values of the control parameter Re$_i$. However, the magni-

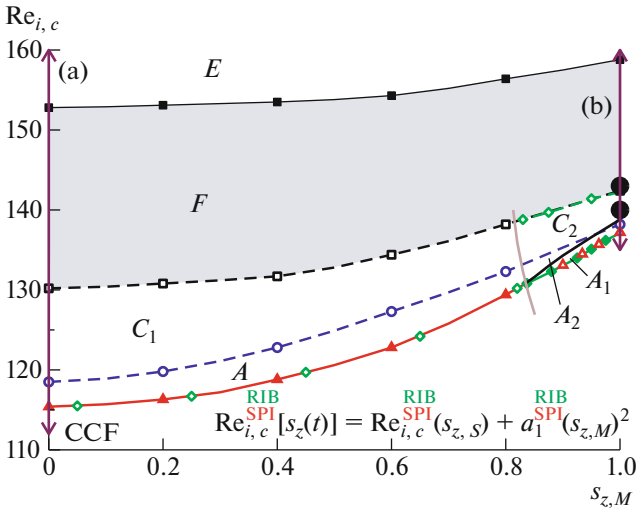

Fig. 7. Phase diagrams.

tude of this effect on the primary bifurcation thresholds is different for SPI/RIB and TVF. For SPI/RIB the stabilization of the CCF basic state can be quantified with an approximate power law according to $\mathrm{Re}_{i,c}^{\mathrm{SPI/RIB}}[s_z(t)]) = \mathrm{Re}_{i,c}^{\mathrm{SPI/RIB},0} + a_1^{\mathrm{SPI/RIB}} s_{z,M}^2$, with $a_1^{\mathrm{SPI/RIB}} = 8$) (Fig. 7). A similar stabilization effect was observed for static magnetic fields [22–24]. However, for TVF the variation (with $s_{z,M}$) under modulated fields is *more complex* and cannot be approximated by such a simple quadratic formula. This is congruent and fits with the former described stronger modifications of the TVF bifurcation branches itself (Fig. 2).

For parameters in Fig. 7 the maximum stability enhancement in Re_i is about 14.6% for SPI/RIB and 16.6% for TVF, comparing the system in absence of any magnetic field with alternating magnetic field at ($s_{z,M} = 1$).

Together with increase in $s_{z,M}$ and stabilization of the CCF basic state also the region (F) of wTVF shrinks in range of Re_i, which will completely disappear, when the primary bifurcation thresholds for SPI and TVF will intersect (cf. [45]) for greater $s_{z,M}$ (out of here presented parameter range).

The thresholds for SPI and RIB are identical [2, 45, 54], while RIB are mostly unstable at onset. While for $s_{z,M} \lesssim 0.82$ SPI appear stable and RIB are unstable at onset, the opposite holds for $s_{z,M} \gtrsim 0.82$. Crossing in the phase space from region F to C_2 one finds the stable connecting branch wTVF–RIB (Fig. 3 (2)), while from region F to C_1 wTVF losses stability and a "jump" bifurcation [44, 45] towards SPI (Fig. 3 (1)) appears.

To summarize, in the terms of stability the system reacts to an alternating modulation of the magnetic field like to an increase in the magnetic field strength in the static case. This holds for all solutions, SPI, RIB, and TVF, while the effect, i.e., the magnitude of stabilization is strongest for SPI/RIB.

Table 1. Various regions, labeled A–D, as presented in the ($\mathrm{Re}_{i,c}, S_{z,M}$) phase space diagrams (Fig. 7), including their stability properties: stable (s), unstable (u), non-existent (–).

Region	A	A_1	A_2	C_1	C_2	D	E	F
TVF	–	–	–	u	u	s	s	u
SPI	s	u	s	s	s	u	s	s
wTVF	–	–	–	–	–	–	–	s
RIB	u	s	s	u	s	u	u	u

SUMMARY

In summary, we have elucidated the consequences onto the flow dynamics of a ferrofluid subject to modulated magnetic field by numerical solutions of the ferro-hydrodynamical equation of motion. Therefore, we considered the Taylor–Couette geometry with counter-rotating cylinders. We showed that modulated magnetic fields stabilize the CCF basic state (moving the bifurcation thresholds to greater values of the control parameters), similar as static fields do. Thereby the stabilization effect, i.e., the magnitude in up-shift, depends on the corresponding solutions, as well as on the control parameters. However, in general the effect seems to be smaller compared with the static case.

The additional frequency Ω_H introduced by the modulated magnetic field has crucial effects on the underlying topology of the flow structures. The main direct result is an *increase in flow complexity* by moving all solutions one step up in the hierarchy of complexity. Thus, TVF, the classical fixed-point solution, becomes a limit cycle (1-torus), while the classical periodic limit-cycle solutions SPI, RIB, and wTVF become quasi-periodic living on a 2-torus invariant manifold. This observation can be interesting for future investigations, e.g., applying such a modulating field onto known 3-tori solutions to see and explore dynamics and potential bifurcation scenarios of potential 4-tori solutions. The latter could get some insight of a new and/or different route towards turbulence (Table 1).

In the here considered high-frequency modulation $\Omega_H = 100$ the ratio between both frequencies of external stimulation and characteristic solution frequencies (wTF, SPI, and RIB) is *not* a rational number, resulting in quasiperiodic response. Only for TVF without such a characteristic frequency we detected subharmonic response. In considering other frequencies Ω_H, e.g., rational multiples of the characteristic ones $f_H = 2f_{\mathrm{SPI}}$ (or $f_H = 2f_{\mathrm{wTVF}}$), interesting resonant phenomena as switching between different modes can be highly expected [34]. Aside, the modulation frequency Ω_H can be also used to control the system to change between the subcritical and supercritical behavior.

Further we detected that for sufficiently strong modulation amplitudes stability is transferred between the two on a common threshold primary bifurcating solutions SPI and RIB. In the corresponding parameter region we could confirm a transition from stable TVF to stable RIB via stable wTVF. This is important as in earlier studies the RIB solution was only found unstable resulting in the phenomenon of "jump bifurcation" [44, 45] to the SPI solution.

Flow control via modulated magnetic field is highly desired for various applications. Based on the here presented findings, interesting work will be the study of variation in driving frequency Ω_H especially with focus in regions with coexisting solutions, e.g., SPI and wTVF.

ACKNOWLEDGMENTS

Sebastian Altmeyer is a Serra Húnter Fellow.

CONFLICT OF INTEREST

The author declares that he has no conflicts of interest.

REFERENCES

1. Taylor, G.I., Stability of a viscous liquid contained between two rotating cylinders, *Phil. Trans. Roy. Soc. London. Ser. A*, 1923, vol. 223, p. 289.
2. Chossat, P. and Iooss, G., *The Couette–Taylor Problem*, Berlin: Springer, 1994.
3. Hu, H.C. and Kelly, R.E., Effect of a time-periodic axial shear flow upon the onset of Taylor vortices, *Phys. Rev. E*, 1995, vol. 51, p. 3242.
4. Marques, F. and Lopez, J., Spacial and temporal resonances in a periodically forced hydrodynamic system, *Physica D. Nonlinear Phenomena,* 2000, vol. 136, p. 340.
5. Weisberg, A., Kevrekidis, I., and Smits, A., Delaying transition in Taylor–Couette flow with axial motion of the inner cylinder, *J. Fluid Mech.*, 1997, vol. 348, p. 141.
6. Murray, B.T., McFadden, G.B., and Coriell, S.R., Stabilization of Taylor–Couette flow due to time-periodic outer cylinder oscillation, *Phys. Fluids A: Fluid Dyn.*, 1990, vol. 2, p. 2147.
7. Donnelly, R., Experiments on the stability of viscous flow between rotating cylinders. III, Enhancement of stability by modulation, *Proc. Roy. Soc. London. Ser. A*, 1964, vol. 281, p. 130.
8. Donnelly, R.F., Reif, F., and Suhl, H., Enhancement of hydrodynamic stability by modulations, *Phys. Rev. Lett.*, 1962, vol. 9, p. 363–365.

9. Ganske, A., Gebhardt, T., and Grossmann, S., Modulation effects along stability border in Taylor–Couette flow, *Phys. Fluids*, 1994, vol. 6, p. 3823.
10. Carmi, S. and Tustaniwskyj, J.I., Stability of modulated finite-gap cylindrical Couette flow: linear theory, *J. Fluid Mech.*, 1981, vol. 108, p. 19.
11. Barenghi, C.F. and Jones, C.A., Modulated Taylor–Couette flow, *J. Fluid Mech.*, 1989, vol. 208, p. 127.
12. Barenghi, C.F., Computations of transitions and Taylor vortices in temporally modulated Taylor–Couette flow, *J. Comput. Phys.*, 1991, vol. 95, p. 175.
13. Rosensweig, R.E., *Ferrohydrodynamics*, Cambridge: Cambridge Univ. Press, 1985.
14. Altmeyer, S., Ferrofluids, *Scholarpedia*, 2020, vol. 15, p. 55163.
15. Altmeyer, S., On the ridge of instability in ferrofluidic Couette flow via alternating magnetic field, *Sci. Reports*, 2021, vol. 11, p. 4705.
16. Neuringer, J.L. and Rosensweig, R.E., Ferrohydrodynamics, *Phys. Fluids*, 1964, vol. 7, p. 1927.
17. Rosensweig, R.E., Kaiser, R., and Miskolczy, G., Magnetoviscosity of magnetic fluid in a magnetic field, *J. Colloid Interface Sci.*, 1969, vol. 29, p. 680.
18. Kashevskii, B.E., On the moment of forces acting on a body in a ferrofluid, *Fluid Dyn.*, 1980, vol. 15, no. 4, pp. 581–585.
19. Niklas, M., Influence of magnetic fields on Taylor vortex formation in magnetic fluids, *Z. Phys. B*, 1987, vol. 68, p. 493.
20. Odenbach, S., Magnetoviscous and viscoelastic effects in ferrofluids, *Int. J. Modern Phys. B*, 2000, vol. 14, p. 1615.
21. Odenbach, S. and Gilly, H., Taylor-vortex flow of magnetic fluids under the influence of an azimuthal magnetic field, *J. Magn. Magn. Mater.*, 1995, vol. 152, p. 123.
22. Reindl M. and Odenbach S., Influence of a homogeneous axial magnetic field on Taylor–Couette flow of ferrofluids with low particle-particle interaction, *Exp. Fluids*, 2011, vol. 50, p. 375.
23. Reindl, M. and Odenbach, S., Effect of axial and transverse magnetic fields on the flow behavior of ferrofluids featuring different levels of interparticle interaction, *Phys. Fluids*, 2011, vol. 23, p. 093102.
24. Altmeyer, S., Hoffmann, C., Leschhorn, A., and Lücke, M., Influence of homogeneous magnetic fields on the flow of a ferrofluid in the Taylor–Couette system, *Phys. Rev. E*, 2010, vol. 82, p. 016321.
25. Altmeyer, S., Lopez, J., and Do, Y., Influence of an inhomogeneous internal magnetic field on the flow dynamics of ferrofluid between differentially rotating cylinders, *Phys. Rev. E*, 2012, vol. 85, p. 066314.
26. Altmeyer, S., Leschhorn, A., Hoffmann, C., and Lücke, M., Elongational flow effects on the vortex growth out of Couette flow in ferrofluids, *Phys. Rev. E*, 2013, vol. 87, p. 053010.
27. Altmeyer, S., Lopez, J., and Do, Y., Effect of elongational flow on ferrofuids under a magnetic field, *Phys. Rev. E*, 2013, vol. 88, p. 013003.
28. Potanin, E.P., Effect of a magnetic field on the circulation of a conductive medium within a rotating cylinder in the presence of a retarding end surface, *Fluid Dyn.*, 2015, vol. 50, no. 5, pp. 672–680.
29. Storozhenkova, A., Stannariusb, R., Tantsyuraa, A.O., and Shabanova, I.A., Measurement of the torque on diluted ferrofluid samples in rotating magnetic fields, *J. Magn. Magn. Mater.*, 2016, vol. 431, p. 66.
30. Altmeyer, S., Agglomeration effects in rotating ferrofluids, *J. Magn. Magn. Mater.*, 2019, vol. 482, p. 239.
31. Shliomis, M.I. and Morozov, K.I., Negative viscosity of ferrofluid under alternating magnetic field, *Phys. Fluids*, 1994, vol. 6, p. 2855.
32. Rosensweig, R., Heating magnetic fluid with alternating magnetic field, *J. Magn. Magn. Mater.*, 2002, vol. 252, p. 370.
33. Goharkhah, M., Salarian, A., Ashjaee, M., and Shahabadi, M., Convective heat transfer characteristics of magnetite nanofluid under the influence of constant and alternating magnetic field, *Powder Technol.*, 2015, vol. 274, p. 258.
34. Smorodin, B.L. and Lücke, M., Convection in binary fluid mixtures with modulated heating, *Phys. Rev. E*, 2009, vol. 79, p. 026315.
35. Smorodin, B.L., The onset of convection of a poorly conducting fluid in a modulated thermal field, *J. Exp. Theor. Phys.*, 2001, vol. 93, no. 6, pp. 1231–1238.
36. Rosenblat, S. and Tanaka, G.A., Modulation of thermal convection instability, *Phys. Fluids*, 1971, vol. 14, p. 1319.
37. Shliomis, M.I., Smorodin, B.L., and Kamiyama, S., The onset of thermomagnetic convection in stratified ferrofluids, *Phil. Mag.*, 2003, vol. 83, nos. 17–18, pp. 2139–2153.
38. Ruuge, E.K. and Rusetski, A.N., Magnetic fluids as drug carriers: Targeted transport of drugs by a magnetic field, *J. Magn. Magn. Mater.*, 1993, vol. 122, p. 335.
39. Chan, D.C.F., Kirpotin, D.B., and Bunn P.A., Synthesis and evaluation of colloidal magnetic iron oxides for the site-specific radiofrequency-induced hyperthermia of cancer, *J. Magn. Magn. Mater.*, 1993, vol. 122, p. 374.

40. Andereck, C.D., Liu, S.S., and Swinney, H.L., Flow regimes in a circular Couette system with independently rotating cylinders, *J. Fluid Mech.*, 1986, vol. 164, p. 155.
41. Tagg, R., The Couette–Taylor problem, *Nonlinear Sci. Today*, 1994, vol. 4, p. 1.
42. Altmeyer, S., Do, Y., Marquez, F., and Lopez, J.M., Symmetry-breaking Hopf bifurcations to 1-, 2-, and 3-tori in small-aspect-ratio counterrotating Taylor–Couette flow, *Phys. Rev. E*, 2012, vol. 86, p. 046316.
43. Altmeyer, S. and Hoffmann, C., On secondary instabilities generating footbridges between spiral vortex flow, *Fluid Dyn. Res.*, 2014, vol. 46, p. 025503.
44. Golubitsky, M., Stewart, I., and Schaeffer, D., *Singularities and Groups in Bifurcation Theory II*, New York: Springer, 1988.
45. Hoffmann, C., Altmeyer, S., Pinter, A., and Lücke, M., Transitions between Taylor vortices and spirals via wavy Taylor vortices and wavy spirals, *New J. Phys.*, 2009, vol. 11, p. 053002.
46. Müller, H.W. and Liu, M., Structure of ferrofluid dynamics, *Phys. Rev. E*, 2001, vol. 64, p. 061405.
47. Langevin, P., Magnétisme et théorie des électrons, *Ann. Chem. Phys.*, 1905, vol. 5, p. 70.
48. Embs, J., Müller, H.W., Wagner, C., Knorr, K., and Lücke, M., Measuring the rotational viscosity of ferrofluids without shear flow, *Phys. Rev. E*, 2000, vol. 61, p. R2196.
49. The specifications for the ferrofluid APG933 are as follows: $\mu_0 M_s = 20$ mT, $\eta P = 0$ mPa, density $\rho = 1.09$ g/cm^3, $\Phi_m = 3.3\%$, susceptibility $\Xi = 0.9$, mean diameter of the particle's magnetic core 10 nm, thickness of the polymeric coating 2 nm."
50. Niklas, M., Müller-Krumbhaar, H., and Lücke, M., Taylor-vortex flow of ferrofluids in the presence of general magnetic fields, *J. Magn. Magn. Mater.*, 1989, vol. 81, p. 29.
51. Odenbach, S. and Müller, H.W., Stationary off-equilibrium magnetization in ferrofluids under rotational and elongational flow, *Phys. Rev. Lett.*, 2002, vol. 89, p. 037202.
52. Altmeyer, S., Leschhorn, A., Hoffmann, C., and Lücke, M., Elongational flow effects on the vortex growth out of Couette flow in ferrofluids, *Phys. Rev. E*, 2013, vol. 87, p. 053010.
53. Swift, J.W. and Wisenfeld, K., Suppression of period doubling in symmetric systems, *Phys. Rev. Lett.*, 1984, vol. 52, p. 705.
54. Demay, Y. and Iooss, G., Calcul des solutions bifurquées pour le problème de Couette–Taylor avec les deux cylindres en rotation, *J. Méc. Théor. Appl.*, 1984, pp. 193–216.
55. Belyaev, A.V. and Smorodin, B.L., Convection of a ferrofluid in an alternating magnetic field, *J. Appl. Mech. Techn. Phys.*, 2009, vol. 50, no. 4, pp. 558–565.